Many-body localization in a quantum simulator with programmable random disorder

J. Smith[1]*, A. Lee[1], P. Richerme[2], B. Neyenhuis[1], P. W. Hess[1], P. Hauke[3,4], M. Heyl[3,4,5], D. A. Huse[6] and C. Monroe[1]

When a system thermalizes it loses all memory of its initial conditions. Even within a closed quantum system, subsystems usually thermalize using the rest of the system as a heat bath. Exceptions to quantum thermalization have been observed, but typically require inherent symmetries[1,2] or noninteracting particles in the presence of static disorder[3–6]. However, for strong interactions and high excitation energy there are cases, known as many-body localization (MBL), where disordered quantum systems can fail to thermalize[7–10]. We experimentally generate MBL states by applying an Ising Hamiltonian with long-range interactions and programmable random disorder to ten spins initialized far from equilibrium. Using experimental and numerical methods we observe the essential signatures of MBL: initial-state memory retention, Poissonian distributed energy level spacings, and evidence of long-time entanglement growth. Our platform can be scaled to more spins, where a detailed modelling of MBL becomes impossible.

It is exceedingly rare in nature for systems to localize, or retain local information about their initial conditions at long times. In an important counterexample, Anderson demonstrated that localization can arise due to the presence of disorder, which can destructively scatter propagating waves and prevent transport of energy or particles[3]. Although this interference effect can be applied to generic quantum systems, most experimental work has been restricted to the narrow parameter regime of low excitation energies and no interparticle interactions[4–6].

Whether such localization persists in the more general case of arbitrary excitation energy and non-zero interparticle interactions was theoretically explored by Anderson[3], and more recently by others[7–10]. This MBL phase is predicted to emerge for a broad set of interaction ranges and disorder strengths, although the precise phase diagram is not well known[11] because equilibrium statistical mechanics breaks down in the MBL phase and numerical simulations are limited to ∼20 particles[8,9]. Very recent experiments searching for MBL have measured constrained mass transport and the breakdown of ergodicity in disordered atomic systems with interactions[12,13].

Here we report the direct observation of MBL in a long-range transverse field Ising model with programmable, random disorder. This is a non-integrable model that cannot be mapped to noninteracting particles (a necessary condition for MBL[7]) and we can easily tune the disorder strength and interaction range over a parameter space that exhibits this phenomenon. Our experiment is effectively a closed quantum system over the timescales of interest, because the system localizes approximately 60 times faster than the coupling rate to the outside environment (see Supplementary Information).

Each of the effective spin-1/2 particles is encoded in the ${}^2S_{1/2}\,|F=0, m_F=0\rangle$ and $|F=1, m_F=0\rangle$ hyperfine 'clock' states of a ${}^{171}Yb^+$ ion, denoted $|\downarrow\rangle_z$ and $|\uparrow\rangle_z$, respectively. We confine a chain of ten ions in a linear radiofrequency Paul trap and apply optical dipole forces to generate the effective spin–spin coupling[14] of a disordered Ising Hamiltonian:

$$H_{\mathrm{Ising}} = \sum_{i<j} J_{i,j}\sigma_i^x\sigma_j^x + \frac{B}{2}\sum_i \sigma_i^z + \sum_i \frac{D_i}{2}\sigma_i^z \qquad (1)$$

where σ_i^γ $(\gamma = x, z)$ are the Pauli matrices acting on the ith spin, $J_{i,j}$ is the coupling strength between spins i and j, B is a uniform effective transverse field, D_i is a site-dependent disordered potential, and $\hbar = 1$ (see Supplementary Information). After the chain evolves for some time, we collect the state-dependent fluorescence on an intensified charge-coupled device camera for site-resolved imaging. This, in addition to our ability to perform high-fidelity rotations, allows measurement of the single-site magnetization $\langle\sigma_i^\gamma\rangle(\gamma = x, y, z)$ as well as arbitrary spin correlation functions along any direction.

$J_{i,j}$ is a tunable, long-range coupling that falls off approximately algebraically as $J_{i,j} \propto J_{\max}/|i-j|^\alpha$ (ref. 15), where $J_{\max}$ is typically 2π (0.5 kHz). Here, we tune α between 0.95 and 1.81, although for most of the data $\alpha \approx 1.13$. We directly measure the complete spin–spin coupling matrix (Fig. 1a), demonstrating the long-range interactions required to exhibit MBL in this model. Moreover, it has been shown numerically that (1) exhibits MBL for the experimental parameters[16].

The site-specific programmable disorder term D_i is sampled from a uniform random distribution with $D_i \in [-W, W]$, where W characterizes the strength of the disorder. The disorder is generated by site-dependent laser-induced Stark shifts (see Supplementary Information), which also allow for preparation of the system into any desired product state. To ensure we observe the general behaviour of the disordered Hamiltonian, we average over 30 distinct random instances of disorder (Fig. 1b,c), which leads to a sampling error that is smaller than the features of interest (see Supplementary Information).

An important signature of the MBL phase is manifested in the spectral statistics of adjacent energy levels of the Hamiltonian. In the thermalizing phase, the energy levels are given by the eigenvalues of a random matrix, a matrix whose elements are given by a random

[1]Joint Quantum Institute, University of Maryland, Department of Physics and National Institute of Standards and Technology, College Park, Maryland 20742, USA. [2]Department of Physics, Indiana University, Bloomington, Indiana 47405, USA. [3]Institute for Quantum Optics and Quantum Information of the Austrian Academy of Sciences, 6020 Innsbruck, Austria. [4]Institute for Theoretical Physics, University of Innsbruck, 6020 Innsbruck, Austria. [5]Physik Department, Technische Universität München, 85747 Garching, Germany. [6]Physics Department, Princeton University, Princeton, New Jersey 08544, USA. *e-mail: htimsjacob@gmail.com

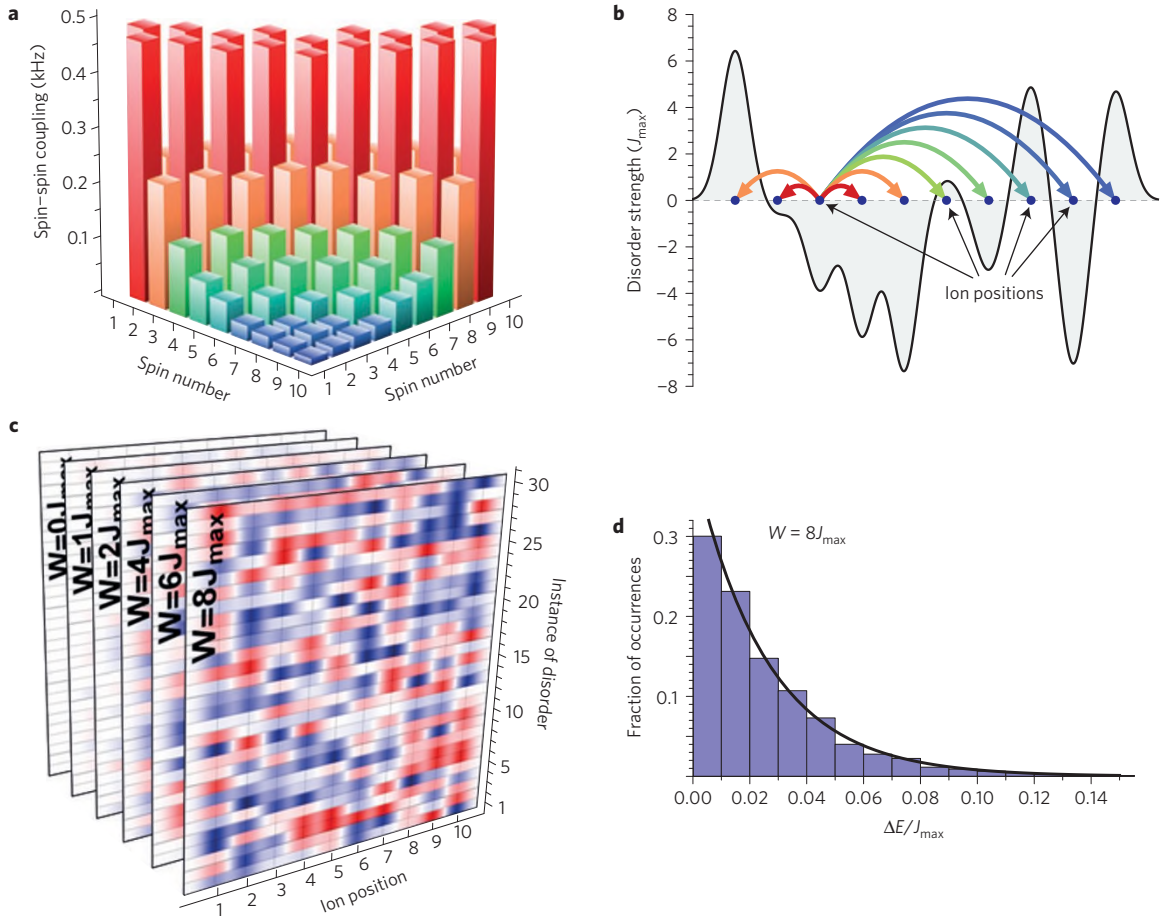

Figure 1 | An interacting spin model with random disorder. a, Directly measured elements of the spin–spin coupling matrix J_{ij}, equation (1) (increasing interaction strength from blue to red). The long-range interactions decay as $J_{max}/r^{1.13}$. **b**, A specific instance of the random disordered field with a schematic illustration of the long-range interactions. **c**, Random values of the disordered field for all 30 instances of disorder for several different disorder strengths and for each ion (red indicates positive values and blue indicates negative values, with values between −0.5 and 0.5). **d**, Level statistics calculated from the measured spin–spin coupling matrix in **a** and applied disorders in **c** are Poisson-distributed (black line is the expected level spacings for a Poisson distribution), as predicted for a MBL system.

distribution, due to level repulsion. However, in the MBL phase, this level repulsion is greatly suppressed because eigenstates typically differ by multiple spins flips. As a result, the level spacing between adjacent energy eigenvalues are Poisson-distributed[8,9]. Using our directly measured spin–spin couplings and applied realizations for the strongest experimental disorder $W = 8J_{max}$ and $B = 4J_{max}$, we calculate the distribution of adjacent energy level splittings and find them to be Poisson-distributed, as expected for a MBL state (Fig. 1d).

Before searching for evidence of localization in the system's time evolution, we first find parameters that cause the measured state to thermalize in the absence of disorder. We increase the transverse field B and look for conditions that result in the single-site magnetization along two orthogonal directions approaching and remaining at their thermal equilibrium values (see Supplementary Information).

Figure 2a shows the measured dynamics of $\langle \sigma_i^z \rangle$ for $B = 4J_{max}$ and $D_i = 0$ with the spins initialized in the Néel ordered state, $|\uparrow\downarrow\uparrow\downarrow\uparrow\downarrow\uparrow\downarrow\uparrow\downarrow\rangle_z$ along the z direction. This configuration has an energy equivalent to an infinite temperature thermal state, because the expectation value of the Hamiltonian is zero. At long times, each expectation value $\langle \sigma_i^z \rangle$ approaches zero, losing memory of the initial ordering. As the transverse field B is increased, the system appears to thermalize more quickly and the level statistics approach those of random matrices rather than Poissonians, as expected for a generic thermodynamic system (see Supplementary Information).

When $B \gg J$, the Hamiltonian is effectively an XY model[17,18] and conserves $\sum_i \sigma_i^z$, because Ising processes that flip spins along the large field are energetically forbidden. Thus, being in a spin configuration with half of the spins up and half of the spins down maximizes the accessible energy states. In addition, the Néel state is never an eigenstate, even for $B \gg J$ and $W \gg J$, because the uniform B field at each site still allows spin exchange in the z-basis.

If a system is thermal, the Eigenstate Thermalization Hypothesis (ETH) provides a general framework where observables reach the value predicted by the microcanonical ensemble[19–21]. This allows us to calculate the expected thermal value of the reduced density matrix given the Hamiltonian and an initial state (see Supplementary Information). To further establish that the system is thermalizing, we measure the reduced density matrix for each spin, $\rho_i = \mathrm{Tr}_{\{j \neq i\}} \rho$, without applied disorder and $B = 4J_{max}$, as shown in Fig. 2a. In our experiment, the spins are initially prepared in a product state with high fidelity. However, at long times, the measured reduced density matrices show that each of the spins is very close to the zero magnetization mixed state, implying the system has locally thermalized.

We apply the random disordered potential, $D_i \neq 0$, with $B = 4J_{max}$ and observe the emergence of MBL as we increase the strength of disorder. Because the many-body eigenstates in the MBL phase are not thermal, transport of energy and spins is suppressed, and ETH fails. Thus, observables will not relax to their thermal

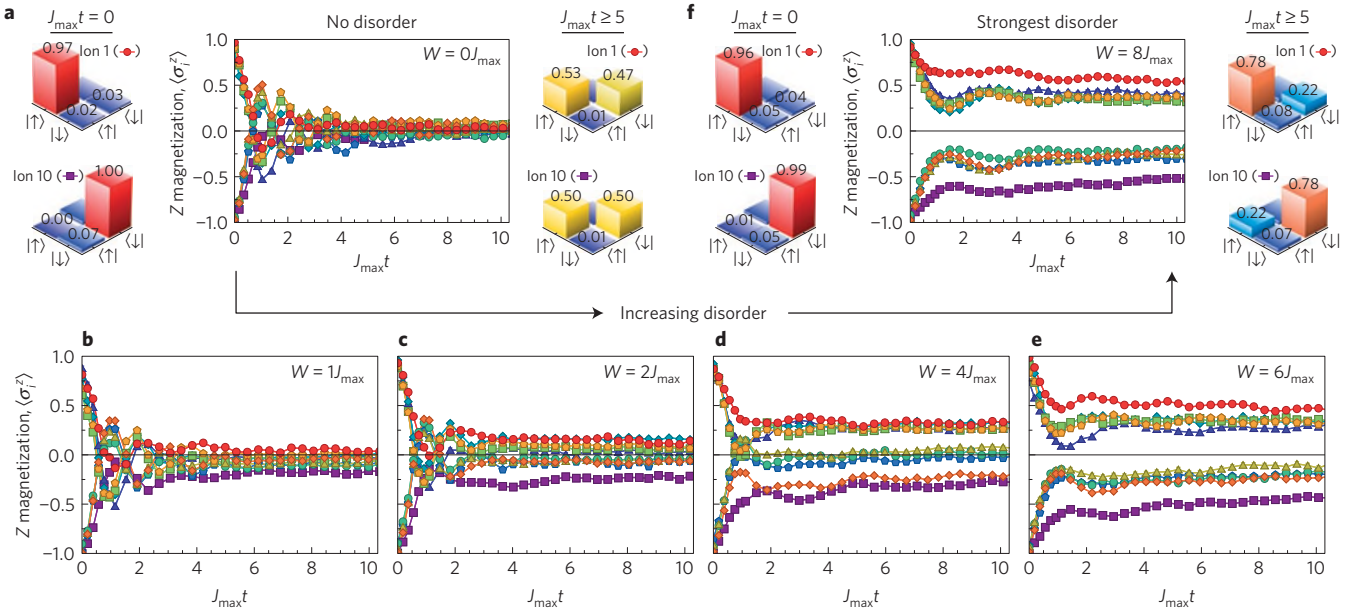

Figure 2 | Emergence of a MBL state. a, Time-evolved single-site magnetizations $\langle\sigma_i^z\rangle$ (different colours represent different ions) for the Hamiltonian in equation (1) for $B = 4J_{max}$ with no applied disorder ($D_i = 0$). The initial-state reduced density matrices for ions 1 and 10 show the spins start in a product state along the z direction. The time-averaged reduced density matrices for $J_{max}t > 5$ (colours from blue to red indicate increasing values of the elements of the density matrix) agree with the values predicted by the ETH, implying the system has thermalized locally. **b**–**e**, As the disorder strength increases, the spins retain more information about their initial state, indicating a transition towards MBL. **f**, Dynamics of $\langle\sigma_i^z\rangle$ for the strongest applied disorder, $W = 8J_{max}$. The initial-state and steady-state time-averaged reduced density matrices for ions 1 and 10 now show that information is preserved about the initial spin configuration at the end of the evolution. Statistical error bars (1 s.d.) are smaller than the data points.

values[9] and memory of the initial conditions will be evident in the single-site magnetization. When starting in the Néel ordered state, Fig. 2b–f shows the time evolution of $\langle\sigma_i^z\rangle$ for different disorder strengths. The frozen moments of the spins increase with increasing disorder as the emergent integrals of motion become more strongly localized[10].

With the maximum applied disorder, $W = 8J_{max}$, we measure the single-spin reduced density matrix for the initial state and the averaged matrix for $J_{max}t \geq 5$. In this case, localization of the spins leads to a marked difference in the measured and thermal reduced density matrices, indicating memory of the system's initial conditions and a breakdown of ETH.

To quantify the localization, we measure the normalized Hamming distance (HD)[22]:

$$\mathcal{D}(t) = \frac{1}{2} - \frac{1}{2N}\sum_i \langle\psi_0|\,\sigma_i^z(t)\sigma_i^z(0)\,|\psi_0\rangle \qquad (2)$$

which gives the number of spin flips away from the initial state, ψ_0, normalized by the length of the chain, N. At long times, the HD approaches 0.5 for a thermalizing state and remains at 0 for a fully localized state. In Fig. 3a, we measure that the long-time HD is 0.5 in the absence of disorder, and becomes smaller as the disorder strength is increased and the system more strongly localizes. This time evolution agrees with exact diagonalization numerical calculations for (1) (see Supplementary Information).

Figure 3b shows that for finite but weak disorder, the time-averaged HD for $J_{max}t > 5$ is essentially unchanged, indicating weak or no localization. However, once the random field is sufficiently strong we observe a crossover from a thermalizing to a localized state. Once in this regime, the system becomes more localized with increasing disorder strength.

There is great theoretical interest in mapping the MBL phase diagram with respect to interaction range and disorder strength[11,22,23]. We have taken the first steps towards this goal

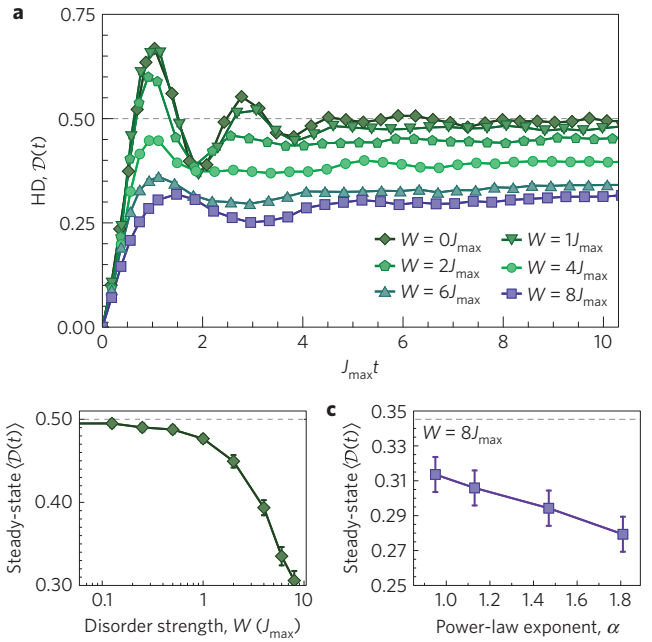

Figure 3 | The Hamming distance (HD). a, The HD exhibits time dynamics that reach their steady-state values after $J_{max}t \approx 5$. For increasing disorder, the system becomes more strongly localized, and the steady-state HD decreases. (Different colours represent different disorder strengths.) **b**, The steady-state HD with respect to the strength of the random potential indicates the state is not or only weakly localized for small disorder, but after the random field is sufficiently strong it becomes more localized with increased disorder. **c**, The steady-state HD with respect to the power-law exponent indicates that the system becomes less localized in the presence of longer-range interactions (smaller α). Error bars, 1 s.d.

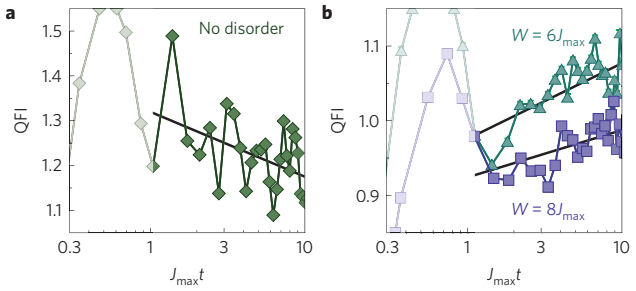

Figure 4 | Quantum Fisher information (QFI). a, Time evolution of the QFI for no disorder, which is consistent with no long-time growth of entanglement. The greyed-out area indicates the fast initial growth of QFI that follows a Lieb–Robinson-type bound. **b**, Long-time logarithmic growth of the QFI for the applied disorder of $W = (6, 8)J_{max}$ is a lower bound for the entanglement in the system and is consistent with the expected long-time growth of entanglement in the MBL state. Black lines are logarithmic fits to the data. Statistical error bars (1 s.d.) are smaller than the data points.

by measuring a change in the time-averaged HD for $W = 8J_{max}$ and $J_{max}t > 5$ as we adjusted the interaction range, $0.95 < \alpha < 1.81$ (Fig. 3c). For shorter-range interactions, the system appears more localized, because the state approaches a fully localized Anderson insulator as $\alpha \to \infty$. This change in time-averaged HD with a change in interaction range makes clear that the long-range couplings are playing a role in the observed dynamics, thus indicating the observed effect is a many-body phenomenon.

Although there are predictions of a many-body delocalization transition at $\alpha = 1.5$ (ref. 23), we did not observe this effect as we tuned α across this boundary. The lack of a sharp transition, along with the presence of MBL states for $\alpha < 1$, may be due to finite size effects (see Supplementary Information). As this system is scaled to many dozens of spins, it will allow better study of the phase transition and mapping of the phase boundary in a regime where numerics are intractable.

A hallmark of MBL is the characteristic growth of entanglement under coherent time evolution[24], although its experimental observation has been elusive so far. In Anderson insulators without many-body interactions, the entanglement production from weakly entangled initial states shows a quick saturation after a sharp transient regime. However, in MBL systems a long-time growth sets in, which is logarithmically slow for short-range interactions[25] and can become algebraic with power-law interactions[26].

This entanglement growth can be measured using a suitable witness operator or even full state tomography[27]. We instead indirectly characterize the entanglement growth in this system by measuring the quantum Fisher information (QFI)[28–30]. The QFI gives a lower bound on the entanglement in the system while requiring only a measurement of two-body correlators, which can be efficiently accessed with our site-resolved imaging. Importantly, the QFI is able to distinguish MBL from single particle localization through the anticipated characteristic entanglement growth (see Supplementary Information). With no applied disorder, we observe a fast initial growth of the QFI following a Lieb–Robinson bound[17,18] as the correlations propagate through the system, but no further growth afterwards (Fig. 4a). In contrast, for the cases of applied disorder of $W = 6J_{max}$ and $W = 8J_{max}$, the further growth of the QFI is consistent with a logarithmic increase of entanglement at long times in a MBL state (Fig. 4b), but absent for single particle localized systems.

Our experimental platform is well suited for studying deep and intractable questions about thermalization and localization in quantum many-body systems. Moreover, the high degree of control in our experiment may guide the use of MBL states as potential quantum memories in naturally disordered quantum systems[24].

Data availability. The data that support the plots within this paper and other findings of this study are available from the corresponding author upon reasonable request.

References

1. Kinoshita, T., Wenger, T. & Weiss, D. S. A quantum Newton's cradle. *Nature* **440,** 900–903 (2006).
2. Gring, M. *et al*. Relaxation and prethermalization in an isolated quantum system. *Science* **337,** 1318–1322 (2012).
3. Anderson, P. W. Absence of diffusion in certain random lattices. *Phys. Rev.* **109,** 1492–1505 (1958).
4. Wiersma, D. S., Bartolini, P., Lagendijk, A. & Righini, R. Localization of light in a disordered medium. *Nature* **390,** 671–673 (1997).
5. Billy, J. *et al*. Direct observation of Anderson localization of matter waves in a controlled disorder. *Nature* **453,** 891–894 (2008).
6. Roati, G. *et al*. Anderson localization of a non-interacting Bose–Einstein condensate. *Nature* **453,** 895–898 (2008).
7. Basko, D. M., Aleiner, I. L. & Altshuler, B. L. Possible experimental manifestations of the many-body localization. *Phys. Rev. B* **76,** 052203 (2007).
8. Oganesyan, V. & Huse, D. A. Localization of interacting fermions at high temperature. *Phys. Rev. B* **75,** 155111 (2007).
9. Pal, A. & Huse, D. A. Many-body localization phase transition. *Phys. Rev. B* **82,** 174411 (2010).
10. Serbyn, M., Papić, Z. & Abanin, D. A. Local conservation laws and the structure of the many-body localized states. *Phys. Rev. Lett.* **111,** 127201 (2013).
11. Yao, N. *et al*. Many-body localization in dipolar systems. *Phys. Rev. Lett.* **113,** 243002 (2014).
12. Kondov, S., McGehee, W., Xu, W. & DeMarco, B. Disorder-induced localization in a strongly correlated atomic hubbard gas. *Phys. Rev. Lett.* **114,** 083002 (2015).
13. Schreiber, M. *et al*. Observation of many-body localization of interacting fermions in a quasi-random optical lattice. *Science* **349,** 842–845 (2015).
14. Mølmer, K. & Sørensen, A. Multiparticle entanglement of hot trapped ions. *Phys. Rev. Lett.* **82,** 1835–1838 (1999).
15. Islam, R. *et al*. Emergence and frustration of magnetism with variable-range interactions in a quantum simulator. *Science* **340,** 583–587 (2013).
16. Wu, Y.-L. & Das Sarma, S. Understanding analog quantum simulation dynamics in coupled ion-trap qubits. *Phys. Rev. A* **93,** 022332 (2016).
17. Richerme, P. *et al*. Non-local propagation of correlations in quantum systems with long-range interactions. *Nature* **511,** 198–201 (2014).
18. Jurcevic, P. *et al*. Quasiparticle engineering and entanglement propagation in a quantum many-body system. *Nature* **511,** 202–205 (2014).
19. Deutsch, J. M. Quantum statistical mechanics in a closed system. *Phys. Rev. A* **43,** 2046–2049 (1991).
20. Srednicki, M. Chaos and quantum thermalization. *Phys. Rev. E* **50,** 888–901 (1994).
21. Rigol, M., Dunjko, V. & Olshanii, M. Thermalization and its mechanism for generic isolated quantum systems. *Nature* **452,** 854–858 (2008).
22. Hauke, P. & Heyl, M. Many-body localization and quantum ergodicity in disordered long-range Ising models. *Phys. Rev. B* **92,** 134204 (2015).
23. Burin, A. L. Localization in a random XY model with long-range interactions: intermediate case between single-particle and many-body problems. *Phys. Rev. B* **92,** 104428 (2015).
24. Nandkishore, R. & Huse, D. A. Many-body localization and thermalization in quantum statistical mechanics. *Annu. Rev. Condens. Matter Phys.* **6,** 15–38 (2015).
25. Bardarson, J. H., Pollmann, F. & Moore, J. E. Unbounded growth of entanglement in models of many-body localization. *Phys. Rev. Lett.* **109,** 017202 (2012).
26. Pino, M. Entanglement growth in many-body localized systems with long-range interactions. *Phys. Rev. B* **90,** 174204 (2014).
27. Haeffner, H. *et al*. Scalable multiparticle entanglement of trapped ions. *Nature* **438,** 643–646 (2005).
28. Helstrom, C. W. *Quantum Detection and Estimation Theory* (Academic, 1976).
29. Braunstein, S. L. & Caves, C. M. Statistical distance and the geometry of quantum states. *Phys. Rev. Lett.* **72,** 3439–3443 (1994).
30. Pezzé, L. & Smerzi, A. in *Proc. Int. School Phys.* (eds Tino, G. & Kasevich, M.) 691–741 (IOS Press, 2014).

Acknowledgements

We thank L. Duan, Z.-X. Gong, T. Grover, C. Laumann, S. Wang, N. Yao and J. Zhang for helpful discussions. This work is supported by the ARO Atomic and Molecular Physics Program, the AFOSR MURI on Quantum Measurement and Verification, the IARPA MQCO Program, and the NSF Physics Frontier Center at JQI. M.H. acknowledges the

Deutsche Akademie der Naturforscher Leopoldina (grant No. LPDS 2013-07 and LPDR 2015-01) and P.H. acknowledges the EU IP SIQS, the SFB FoQuS (FWF Project No. F4016-N23) and the ERC synergy grant UQUAM.

Author contributions

J.S., A.L., P.R., B.N., P.W.H. and C.M. performed the experimental work and P.H., M.H. and D.A.H. performed the theoretical work. All authors contributed to the preparation of this manuscript.

Additional information

Supplementary information is available in the online version of the paper. Reprints and permissions information is available online at www.nature.com/reprints. Correspondence and requests for materials should be addressed to J.S.

Competing financial interests

The authors declare no competing financial interests.